

## 3D-QSAR and molecular docking studies on pyrazolopyrimidine derivatives as glycogen synthase kinase-3 $\beta$ inhibitors

Nigus Dessalew, Dhilon S. Patel, Prasad V. Bharatam \*

Department of Medicinal Chemistry, National Institute of Pharmaceutical Education and Research (NIPER),  
S.A.S. Nagar (Mohali), 160 062 Punjab, India

Received 8 May 2006; received in revised form 28 August 2006; accepted 29 August 2006  
Available online 3 September 2006

### Abstract

Glycogen synthase kinase-3 (GSK-3), a serine/threonine kinase, is a fascinating enzyme with diverse biological actions in intracellular signaling systems, making it an emerging target for diseases such as diabetes mellitus, cancer, chronic inflammation, bipolar disorders and Alzheimer's disease. It is important to inhibit GSK-3 selectively and the net effect of the GSK-3 inhibitors thus should be target specific, over other phylogenetically related kinases such as CDK-2. In the present work, we have carried out three-dimensional quantitative structure activity relationship (3D-QSAR) studies on novel class of pyrazolopyrimidine derivatives as GSK-3 inhibitors reported to have improved cellular activity. Docked conformation of the most active molecule in the series, which shows desirable interactions in the receptor, was taken as template for alignment of the molecules. Statistically significant CoMFA and CoMSIA models were generated using 49 molecules in training set. By applying leave-one-out (LOO) cross-validation study,  $r_{cv}^2$  values of 0.53 and 0.48 for CoMFA and CoMSIA, respectively and non-cross-validated ( $r_{ncv}^2$ ) values of 0.98 and 0.92 were obtained for CoMFA and CoMSIA models, respectively. The predictive ability of CoMFA and CoMSIA models was determined using a test set of 12 molecules which gave predictive correlation coefficients ( $r_{pred}^2$ ) of 0.47 and 0.48, respectively, indicating good predictive power. Based upon the information derived from CoMFA and CoMSIA contour maps, we have identified some key features that explain the observed variance in the activity and have been used to design new pyrazolopyrimidine derivatives. The designed molecules showed better binding affinity in terms of estimated docking scores with respect to the already reported systems; hence suggesting that newly designed molecules can be more potent and selective towards GSK-3 $\beta$  inhibition.

© 2006 Elsevier Inc. All rights reserved.

**Keywords:** Glycogen synthase kinase-3 (GSK-3); Diabetes mellitus; Pyrazolopyrimidine; 3D-QSAR; CoMFA; CoMSIA; Molecular docking

### 1. Introduction

Glycogen synthase kinase-3 (GSK-3) was identified in 1980 that phosphorylated and inactivated glycogen synthase (GS), the rate-limiting enzyme of glycogen biosynthesis [1]. Since GSK-3 is ubiquitously expressed *in vivo*, GS remain inactive. On the other hand, insulin, signaling via protein kinase B (PKB) pathway, inhibits GSK-3, resulting in GS activity [2,3]. In addition to GS, GSK-3 also phosphorylates and regulates the functions of many metabolic, signaling and structural proteins like activator protein-1, cyclic AMP response element binding protein, nuclear factor of activated T cells, heat shock factor-1,  $\beta$ -catenin and NF- $\kappa$ B [4]. GSK-3 has recently emerged as key

target for several human diseases such as cancer [5], type-2 diabetes [6], chronic inflammatory processes [7], and neurological diseases such as bipolar disorders [8] or Alzheimer's disease [9].

Inhibition of GSK-3 activity can be achieved through three distinct mechanisms (i) ATP non-competitive (in substrate interaction domain), (ii) ATP competitive (in ATP binding pocket) and (iii) metal ion competitive (in  $Mg^{2+}$  binding site) [10]. ATP non-competitive inhibitors compete with the binding of primed substrates to the enzyme's phosphate interaction site for example Martinez et al. [11] reported 2,4-disubstituted thiadiazolidineones (Fig. 1) to inhibit GSK-3 in an ATP-uncompetitive manner. First generation of the ATP-competitive GSK-3 inhibitors such as hymenialdisine [12], paullones [13], indirubins [14] (Fig. 1), etc., are reported but facing the problem of selectivity for GSK-3. They were reported to have inhibitory activity for CDKs, which are homologous protein

\* Corresponding author. Tel.: +91 172 2214684; fax: +91 172 2214692.

E-mail address: [pvbharatam@niper.ac.in](mailto:pvbharatam@niper.ac.in) (P.V. Bharatam).

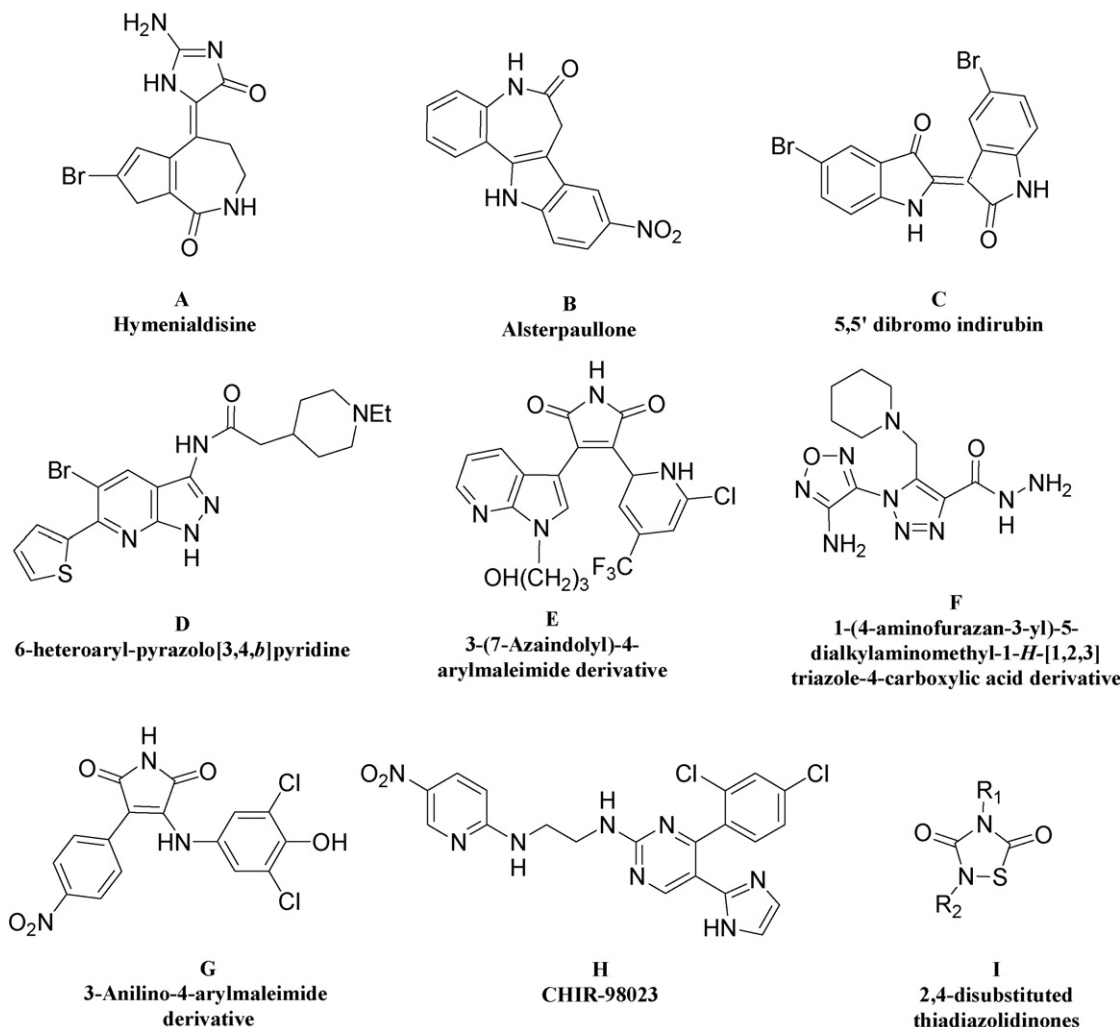


Fig. 1. ATP-competitive (A–H) and ATP non-competitive (I) GSK-3 inhibitors.

kinases to GSK-3. To overcome the problem of selectivity, second generation of ATP-competitive GSK-3 inhibitors like 6-heteroaryl-pyrazolo[3,4-*b*]pyridine [15], 3-(7-azaindolyl)-4-arylmaleimides [16], 1-(4-aminofurazan-3-yl)-5-dialkylaminomethyl-1-*H*-[1,2,3]triazole-4-carboxylic acid derivatives [17], 3-anilino-4-arylmaleimides [18], CHIR98023 [19], etc. were introduced, which show improved selectivity profile for GSK-3. Further modulation of these systems is required to improve selectivity.

Structure-based approaches have been used to provide structural and binding variation based on the interactions shown by selective and non-selective ATP-competitive GSK-3 inhibitors. Several computational approaches were also employed in the development of the above reported selective inhibitors. Recently we proposed a pharmacophore map for selective GSK-3 inhibition and new leads were obtained through virtual screening studies [21a]. We have also employed selective molecular field approach in designing new selective GSK-3 inhibitors [21b]. Several QSAR studies were also reported to explore the structural requirements for GSK-3 inhibitors [20–24]. In this paper we report 3D-QSAR studies using CoMFA [25] and CoMSIA [26] methodologies

on pyrazolopyrimidine derivatives [27]. Partial least square (PLS) [28] based statistical analysis was carried out on aligned molecules to identify the correlation. The contour maps generated help in explaining the observed variation in activity for given structural difference in GSK-3 inhibitors. Important features observed in the developed model have been used to design new molecules, which showed higher predictivity and binding affinity in terms of different binding scores and selectivity in terms of interaction within the GSK-3 $\beta$  active site.

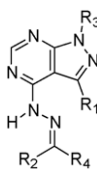
## 2. Computational details

### 2.1. Dataset for analysis

The *in vitro* biological activity data reported as IC<sub>50</sub> for inhibition of GSK-3 $\beta$  by the pyrazolopyrimidine derivatives [27] was used in this study. The IC<sub>50</sub> values were converted to the corresponding pIC<sub>50</sub> values using the formula (pIC<sub>50</sub> = –log IC<sub>50</sub>) (Table 1). A total of 61 molecules were available with pIC<sub>50</sub> values of which 49 molecules were chosen for training set and 12 were selected as a part of test set.

Table 1

Dataset used for 3D-QSAR analysis with corresponding actual and predicted activities



Cpd	R1	R2	R3	R4	Actual pIC <sub>50</sub>	Predicted pIC <sub>50</sub>		Residuals	
						CoMFA	CoMSIA	CoMFA	CoMSIA
1	H	H	–Ph-2-OMe	–4-Pyridyl	5.60	5.69	5.85	–0.09	–0.25
2	H	H	–Ph-4-OMe	–4-Pyridyl	6.00	6.06	6.44	–0.06	–0.44
3	H	H	–Ph-2-OEt	–4-Pyridyl	7.00	7.02	6.88	–0.02	0.12
4	H	H	–Ph-2-OCF <sub>3</sub>	–4-Pyridyl	6.50	6.68	6.50	–0.18	0.00
5	H	H	–Ph-2-NHnPr	–4-Pyridyl	5.40	5.39	5.66	0.01	–0.26
6	H	H	–Ph-2-NH(CH <sub>2</sub> ) <sub>3</sub> cyclopropyl	–4-Pyridyl	5.70	5.72	5.68	–0.02	0.02
7	H	H	–Ph-2-NHAc	–4-Pyridyl	6.80	6.72	6.95	0.08	–0.15
8	H	H	–Ph-3-OMe	–Ph-4-F	8.10	7.97	7.82	0.13	0.28
9	H	H	–Ph-3-OMe	–Ph-4-SO <sub>2</sub> Me	8.60	8.87	8.74	–0.27	–0.14
10	H	H	–Ph-3-OMe	–Ph-4-CO <sub>2</sub> H	7.50	7.79	7.67	–0.29	–0.17
11	H	H	–Ph	–Ph-(3-OMe,4-OH)	7.00	6.95	6.72	0.05	0.28
12	H	H	–Ph-2-NH(CO) <i>n</i> Pr	–4-Pyridyl	6.20	6.12	6.19	0.08	0.01
13	H	H	–Ph-2-F	–4-Pyridyl	6.50	6.44	6.57	0.06	–0.07
14	H	H	–3-pyridyl	–4-Pyridyl	7.50	7.73	7.76	–0.23	–0.26
15	H	H	–4-Pyridyl	–4-Pyridyl	8.50	8.19	8.30	0.31	0.20
16	H	H	–2-pyridyl-3-OMe	–4-Pyridyl	7.40	7.27	7.45	0.13	–0.05
17	H	H	–2-thiazole	–4-Pyridyl	7.40	7.48	7.39	–0.08	0.01
18	H	H	–Ph-3-OMe	–Ph	8.00	7.86	7.83	0.15	0.17
19	H	H	–Ph	–4-Pyridyl	7.00	6.79	7.17	0.21	–0.17
20	H	H	–Ph	–Ph-4-F	6.20	6.76	7.16	–0.56	–0.96
21	H	H	–Ph-3-OMe	–Ph-2-OMe	7.60	7.71	7.59	–0.11	0.01
22	H	H	–Ph-3-OMe	–Ph-4-OMe	7.50	7.72	7.75	–0.22	–0.25
23	H	H	–Ph-3-OMe	–Ph-2-F	6.90	7.09	7.60	–0.19	–0.70
24	H	H	–Ph-3-OMe	–Ph-3-F	8.10	7.92	7.80	0.18	0.30
25	H	H	–Ph-3-OMe	–Ph-3,4-diF	7.80	7.93	7.63	–0.13	0.17
26	H	H	–Ph-3-OMe	–Ph-3-NH <sub>2</sub>	8.00	8.07	7.89	–0.07	0.11
27	H	H	–Ph-3-OMe	–Ph-4-NH <sub>2</sub>	8.60	8.63	8.76	–0.03	–0.16
28	H	H	–Ph-3-OMe	–Ph-2-SO <sub>2</sub> Me	8.40	8.37	8.64	0.03	–0.24
29	H	H	benzimidazole	–Ph-4-F	8.20	8.23	8.24	–0.03	–0.04
30	H	H	benzimidazole	–Ph-4-C(O)NH(CH <sub>2</sub> ) <sub>2</sub> NMe <sub>2</sub>	8.80	8.69	8.82	0.11	–0.02
31	H	H	benzimidazole	–Ph-4-SO <sub>2</sub> Me	8.30	8.18	8.55	0.12	–0.25
32	H	H	benzimidazole	–Ph-4-CO <sub>2</sub> H	8.30	8.16	8.13	0.14	0.17
33	H	H	–Ph-3-OMe	–Ph-4-OH	7.90	7.68	7.71	0.22	0.19
34	H	H	–Ph-3-OMe	–Ph-4-O-allyl	6.80	6.88	6.77	–0.08	0.03
35	H	H	–Ph-3-OMe	–Ph-4-O-Bn-4-F	5.60	5.39	5.20	0.21	0.40
36	H	H	–Ph-3-OMe	–Ph-4-O(CH <sub>2</sub> ) <sub>2</sub> NMe <sub>2</sub>	8.20	8.22	8.02	–0.02	0.18
37	H	H	–Ph-3-OMe	–Ph-4-CH <sub>2</sub> NMe <sub>2</sub>	8.30	8.46	8.20	–0.16	0.10
38	H	H	–Ph-3-OMe	–Ph-4-NHSO <sub>2</sub> Me	7.80	7.86	7.56	–0.07	0.24
39	H	H	–Ph-3-OMe	–Ph-4-NH(CO)(CH <sub>2</sub> ) <sub>2</sub> NMe <sub>2</sub>	8.30	8.08	8.49	0.22	0.19
40	H	V	–Ph-3-OMe	–Ph-4-CN	7.80	7.73	7.67	0.07	0.13
41	Me	H	–Ph-3-OMe	–4-Pyridyl	8.00	8.09	7.95	–0.09	0.05
42	Et	H	–Ph-3-OMe	–4-Pyridyl	7.90	7.83	7.72	0.08	0.18
43	H	H	H	–Ph-(3-OMe,4-OH)	5.50	5.48	5.32	0.02	0.18
44	n-Pr	H	–Ph-3-OMe	–4-Pyridyl	8.00	7.92	7.69	0.08	0.31
45	i-Pr	H	–Ph-3-OMe	–4-Pyridyl	7.50	7.59	7.59	–0.09	–0.09
46	H	Me	–Ph-3-OMe	–4-Pyridyl	7.20	7.41	7.17	–0.21	0.03
47	Me	Me	–Ph-3-OMe	–4-Pyridyl	5.20	5.19	5.50	0.01	–0.30
48	H	H	<i>i</i> -Pr	–Ph-(3-OMe,4-OH)	5.60	5.45	5.64	0.15	–0.04
49	H	H	O-Me	–4-Pyridyl	6.80	6.63	6.25	0.17	0.55
50t	H	H	–Ph-3-Me	–4-Pyridyl	6.80	6.32	6.42	0.48	0.38
51t	H	H	–Ph-3-OMe	–4-Pyridyl	8.20	8.30	7.79	–0.10	0.41
52t	H	H	–Ph-3-OMe	–Ph-4-C(O)NH(CH <sub>2</sub> ) <sub>2</sub> NMe <sub>2</sub>	7.80	8.08	8.49	–0.28	–0.69
53t	H	H	–Ph-3-Br	–4-Pyridyl	6.60	6.52	6.49	0.08	0.11
54t	H	H	–2-Pyridyl	–4-Pyridyl	5.90	6.72	7.24	–0.82	–1.34
55t	H	H	–Ph	–Ph-4-C(O)NH(CH <sub>2</sub> ) <sub>2</sub> NMe <sub>2</sub>	7.70	7.39	7.98	0.31	–0.28

Table 1 (Continued)

Cpd	R1	R2	R3	R4	Actual pIC <sub>50</sub>	Predicted pIC <sub>50</sub>		Residuals	
						CoMFA	CoMSIA	CoMFA	CoMSIA
<b>56t</b>	H	H	benzimidazole	–4-Pyridyl	8.40	8.20	8.24	0.20	0.16
<b>57t</b>	H	H	–Ph-3-OMe	–Ph-4-CH <sub>2</sub> NHEt	8.40	8.15	7.80	0.25	0.60
<b>58t</b>	H	H	–Ph-3-OMe	–Ph-4-NHAc	7.90	9.06	8.23	–1.16	–0.33
<b>59t</b>	H	H	–Ph-3-OMe	–Ph-4-C(O)NH (CH <sub>2</sub> ) <sub>2</sub> SO <sub>2</sub> Me	8.10	7.43	7.93	0.67	0.17
<b>60t</b>	H	H	–Ph-3-OMe	–Ph-4-SO <sub>2</sub> NH (CH <sub>2</sub> ) <sub>2</sub> NMe <sub>2</sub>	8.00	8.73	8.57	–0.73	–0.57
<b>61t</b>	H	H	–Ph	–Ph-(3-OMe,4-OH)	7.00	6.28	6.44	0.72	0.56
<b>62<sup>a</sup></b>	H	H	–Ph-3-OMe	–Ph-4-NEt <sub>2</sub>	5.60	7.90	7.46	–2.30	–1.80

<sup>t</sup> stands for molecules used as a test set molecules.

<sup>a</sup> Stands for the outlier molecule.

Those systems with undefined chirality and vague pIC<sub>50</sub> values are not included in this study.

## 2.2. Conformational search and molecular alignment

Since the crystal structure of the complexes of GSK-3 $\beta$  with pyrazolopyrimidine inhibitors is not reported, the most active molecule **30** from the series is subjected to systematic conformational search with 10<sup>0</sup> increments of all freely rotatable bonds. The global minimum obtained from this search was optimized using MOPAC applying the AM1 [29] Hamiltonian. Other molecules were generated using the conformational of the reference molecule **30** and were minimized by adopting same method. Alignment criterion plays an important role in CoMFA and CoMSIA studies and it is preferable to choose an alignment which maintains the bioactive conformation. In the present study the optimized structures of 61 molecules were aligned on the template molecule **30** by the ALIGN DATABASE command in SYBYL6.9 [30] using the substructure that is common to all (Fig. 2). The resulting alignment is shown in Fig. 3.

## 2.3. 3D-QSAR model generation

The standard Tripos force fields were employed for the CoMFA and CoMSIA analysis. A 3D cubic lattice of dimension 4 Å in each direction with each lattice intersection of regularly spaced grid of 2.0 Å was created. The steric and electrostatic parameters were calculated in case of the CoMFA fields while hydrophobic, acceptor and donor parameters in addition to steric and electrostatic were calculated in case of the CoMSIA fields at each lattice. The sp<sup>3</sup> carbon atom was used as a probe atom to generate steric (Lennard-Jones potential) field energies and a charge of +1 to generate electrostatic (Coulombic potential) field energies. A distance dependent dielectric

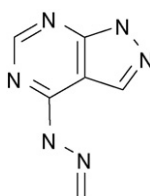


Fig. 2. Common substructure used for alignment.

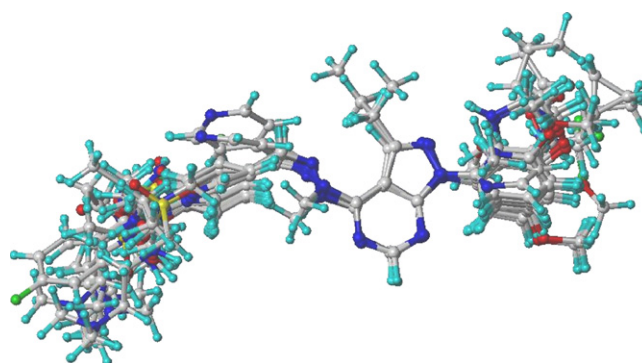


Fig. 3. Alignment of pyrazolopyrimidine derivatives in three dimensions.

constant of 1.00 was used. The steric and electrostatic fields were truncated at +30.00 kcal/mol.

### 2.3.1. Partial least squares (PLS)

Statistical method was used to linearly correlate the CoMFA and CoMSIA fields to the binding affinity values. The cross-validation analysis was performed using leave-one-out (LOO) method. The cross-validated  $r^2$  ( $r_{cv}^2$ ) that resulted in optimum number of components and lowest standard error of prediction were taken. To speed up the analysis and reduce noise, a minimum column filter value  $\sigma$  of 2.00 kcal/mol was used. Final analysis was performed to calculate conventional  $r^2$  ( $r_{ncv}^2$ ) using the optimum number of components obtained from the cross-validation analysis. Since the statistical parameters were found to be the best for the model from the LOO method, it was employed for further predictions of the designed molecules.

## 2.4. Molecular docking

FlexX [31] based molecular docking study was carried out to perform screening and validation of the designed molecules. FlexX method of molecular docking involves incremental construction of ligands from smaller fragments in the cavity of a receptor. All the designed molecules were docked into the ATP binding site in the co-crystal of AMP-PNP, with human GSK-3 $\beta$  enzyme (PDB accession number 1PYX) [20a]. Receptor description file (RDF) was created within the area of 6.9 Å around the co-crystallized ligand. As FlexX ignores HETATM records like metal atom, the bound ligand and the water molecules in the PDB file during docking study, for the

enrichment of the docking study, H-bonding interactions of ligand in hinge region with Val135 and Asp133 were defined as core interactions in the RDF.  $Mg^{2+}$  parameters and conserved water molecule near Thr138 were also defined in RDF. For a comparative analysis of the designed molecules, FlexX score, G\_score [32], PMF\_score [33], D\_score [34] and Chem\_score [35] were estimated using the C-Score module of the Sybyl6.9.

### 3. Results and discussion

#### 3.1. Statistical analysis

The 3D-QSAR, CoMFA and CoMSIA, studies were carried out using pyrazolopyrimidine series of GSK-3 $\beta$  inhibitors reported by Peat et al. [27]. Molecules which do not have bioactivity in exact numerical form for the inhibition of the enzyme were subsequently removed from the analysis. Molecule **62** was found as outlier and removed from the dataset, following this a total of 61 molecules were used for derivation of the models. These were divided into a training set of 49 and a test set of 12 molecules at random with bias given to structural diversity in both the training set and the test set so as to form the standard 4:1 training set to test set ratio for a QSAR study. The way to achieve high selectivity towards GSK-3 $\beta$  has been a difficult one given the diverse substrates this enzyme has and the common mechanism it shares with other phylogenetically related kinases. With this in mind QSAR model of these ATP-competitive inhibitors was built which would account for the biological activity seen in this series and to capitalize upon the insight from the same to design ligands with pronounced inhibitory potency.

The CoMFA and CoMSIA statistical analysis is summarized in Table 2. Statistical data shows  $r_{cv}^2$  0.53 for CoMFA and 0.48 for the CoMSIA models, respectively, which indicates a good internal predictive ability of both models. The models developed also exhibited  $r_{ncv}^2$  of 0.98 and 0.92 for CoMFA and CoMSIA, respectively. To test the predictive ability of the models, a test set of 12 molecules excluded from the model derivation was used. The predictive correlation coefficient  $r_{pred}^2$  of 0.47 for CoMFA and 0.48 for the CoMSIA models indicate good external predictive ability of the model. To this end, a bootstrapping analysis was carried out for 100 runs. Bootstrapping analysis involved further validation of the model by statistical sampling of the original data set to create new data

Table 2  
PLS result summary

Statistical parameters	CoMFA	CoMSIA
$r_{cv}^2$	0.53	0.48
Number of molecules in training set	49	49
Number of molecules in test set	12	12
ONC	8	5
SEE	0.154	0.296
$r^2$	0.98	0.92
$F_{ratio}$	249.174	101.061
$r_{bs}^2$	0.99	0.96
S.D.	0.006	0.019
$r_{pred}^2$	0.47	0.48
Fraction of field contributions		
Steric	0.479	0.120
Electrostatic	0.521	0.273
Hydrophobic	–	0.264
Donor	–	0.199
Acceptor	–	0.144

ONC = optimum number of components, SEE = standard error of estimate, S.D. = standard deviation.

sets. Thus, the difference in the parameters calculated from the original data and the average of the parameters calculated from the  $N(=100)$  runs of bootstrapping sampling is a measure of the bias of the original calculation. This yielded higher  $r_{bs}^2$  value 0.99 for CoMFA and 0.96 for CoMSIA, further supports the statistical validity of the developed models. The graph for the actual and predicted  $pIC_{50}$  values for training set of CoMFA and CoMSIA studies shown in Fig. 4. The histogram of residuals of test set molecules in CoMFA and CoMSIA studies shown in Fig. 5.

#### 3.2. Contour analysis

The contour maps of CoMFA (electrostatic and steric) and CoMSIA (electrostatic, steric, hydrophobic, donor and acceptor) are represented by colour codes shown in Fig. 6. The default level of contour by contribution, 80 for favoured region and 20 for disfavoured region was set during contour analysis. Contour analysis has been performed by dividing total molecular area in to four subdivisions (Fig. 7). There is a defined central core, which is common to all molecules. The aromatic substitution to the N1 of the central core is defined as region A, while substitution to the hydrazone nitrogen was

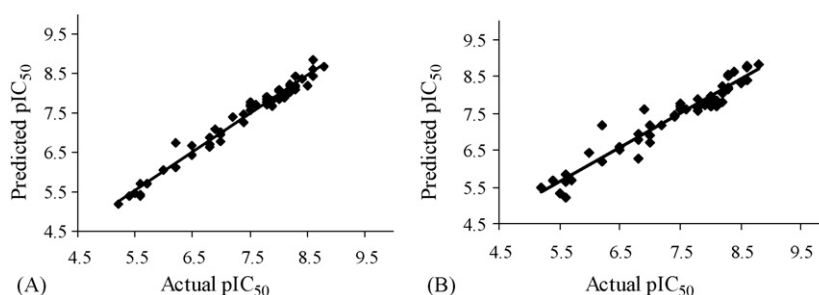


Fig. 4. (A) CoMFA actual vs. predicted  $IC_{50}$  and (B) CoMSIA actual vs. predicted  $IC_{50}$ .



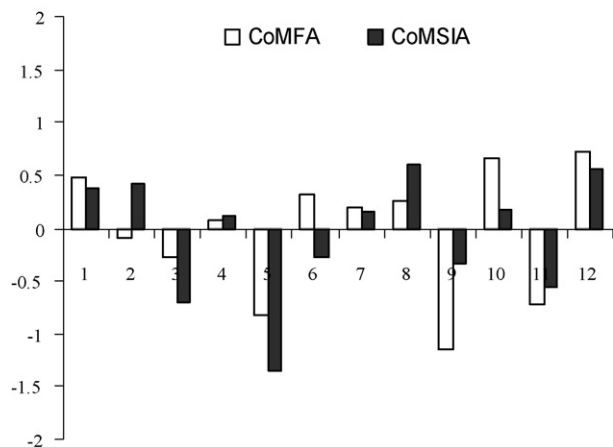


Fig. 5. Histogram of the residuals of the test set molecules.

subdivided into region B (group containing hetero atom) and region C (extended side chain).

### 3.3. Steric contour map

Both CoMSIA and CoMFA steric maps are shown in Fig. 8a and b, respectively. CoMSIA steric map showed green and yellow plots on the opposite planes of the aromatic substitution in region A while CoMFA steric map showed two separated green contours and three small yellow contours in this region. Both CoMSIA and CoMFA steric maps showed a small yellow plot near the C-3 position of central core and another medium sized yellow plot near the side chain substitution to hydrazone moiety in region C. The most active molecule **30** showed benzimidazole substitution in region A, covering the green

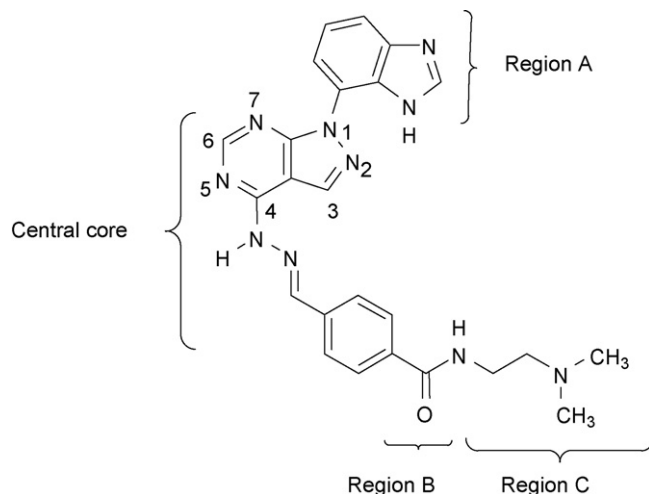


Fig. 7. Most active molecule showing different regions which are used in contour analysis.

contour while NMe<sub>2</sub> side chain substitution is slightly away from yellow contour in region C favourable for binding of the ligand and hence accounts for greater activity of this molecule. Both the CoMSIA and CoMFA steric maps of lower active molecules **1**, **2**, **5**, **6**, etc. showed the conformation of the substituent at N1 position towards the yellow contour in region A which is unfavourable for bulkier substituents. On the other hand better active molecules **56**, **29**, **30**, **31**, **24**, **26**, **27**, **28**, etc. showed the conformation of substituents towards the green plot suggesting favourable steric contributions. Molecules **34** and **35** showed complete incorporation of extended side chain into the big yellow contour present in region C apparently responsible for their lower potency. Molecules **37** and **57** have higher activity due to the absence of the steric clash due to extended side chain substitution in region C. The lower activity of molecules **43** and **48** may be due to the absence of aromatic substitution in region A. Very small yellow plot opposite to C-3 disfavour bulky substituent at this position but it does not give much impact on reduction in activity if there is any bulky substituent. The difference in the activity of **47** and **46** appears to arise from the fact that the methyl at C-3 position of the **47** is oriented towards two small yellow plots and hence is entering unfavourable site, while such unfavourability is absent in the case of **46**.

### 3.4. Electrostatic contour map

CoMSIA and CoMFA electrostatic contour maps are shown in Fig. 8c and d, respectively. CoMSIA electrostatic map showed red contour in region A, which overlaps the aromatic substituent and suggested that increase in ring electronegativity may favour higher activity of molecules, for example, **56**, **29**, **30**, **31**, **32**, **15**, etc. and two small blue contours just opposite to imidazole nitrogen in the same region, where an increase of positive charge is expected to improve the binding affinity of the molecule. CoMFA electrostatic map showed four different red contours in region A, two of which over the plane of

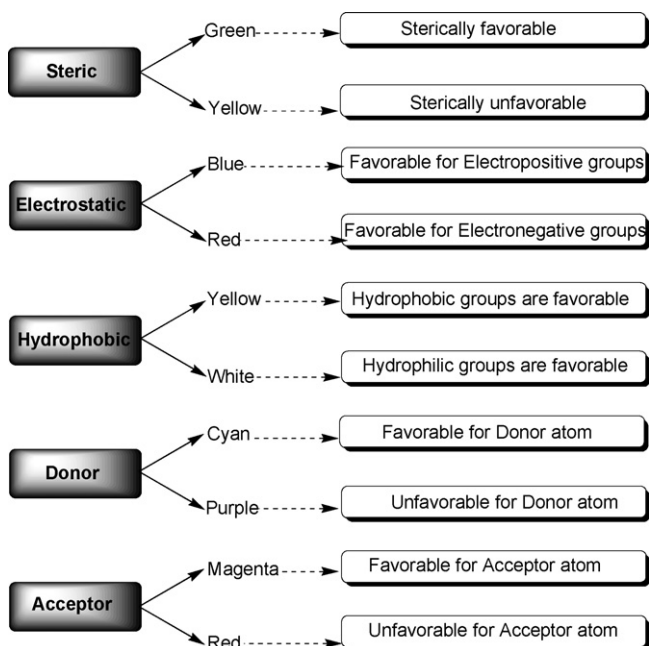


Fig. 6. Colour code representation for CoMFA and CoMSIA contour maps.

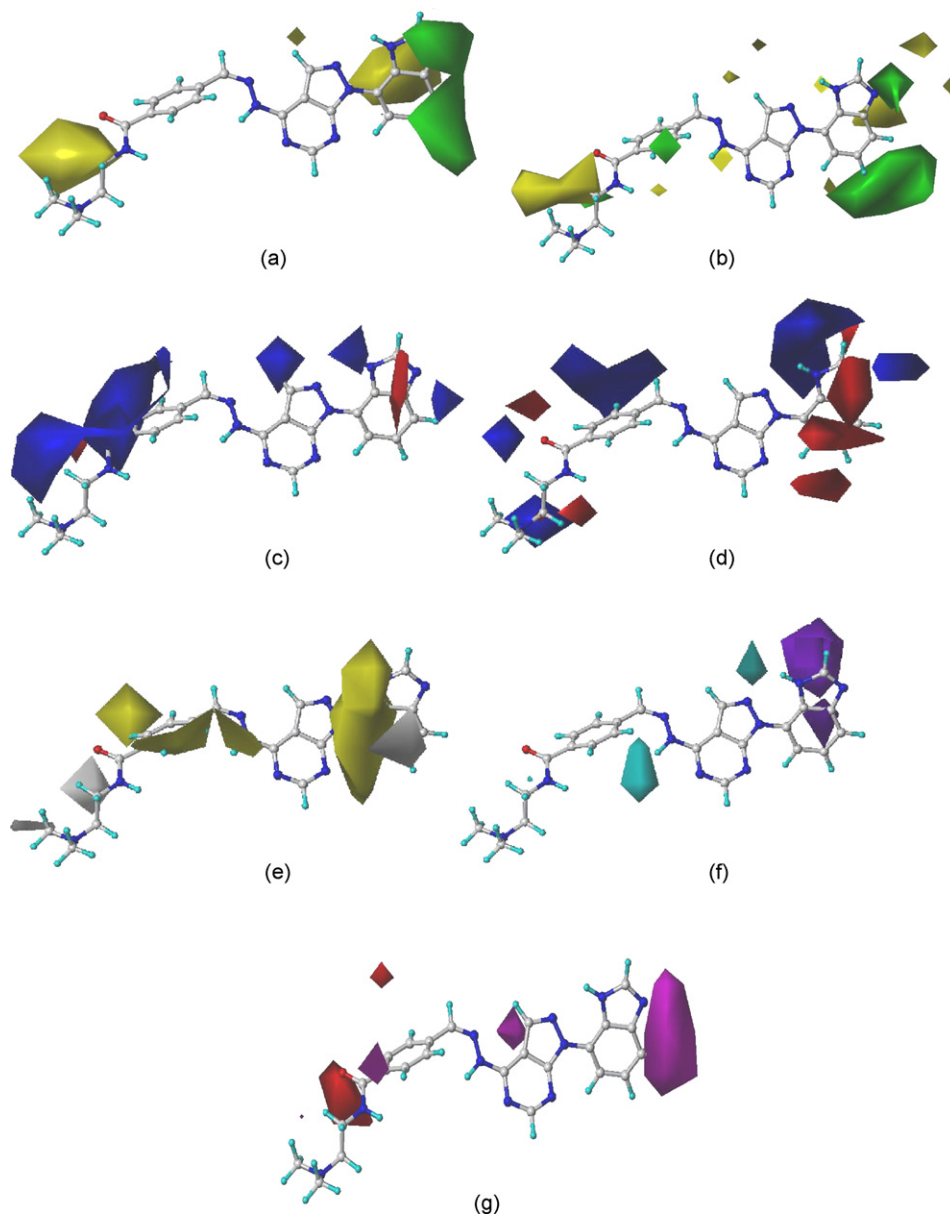


Fig. 8. CoMSIA (steric (a), electrostatic (c), hydrophobic (e), donor (f) and acceptor (g)) contour maps and CoMFA (steric (b) and electrostatic (d)) contour maps around the reference molecule **30**.

aromatic substitution support the favourability of ring electronegativity and other two red contours beside the aromatic substitution also corroborate the favourability of partial negative charge in this region. Two blue plots are found in region A similar to that in CoMSIA electrostatic map. CoMSIA electrostatic map shows a small blue plot near the hydrogen at C-3 position of central core suggesting the substitution of electropositive group at this position to favour the binding of the molecule to the protein, while CoMFA electrostatic map does not show any blue contour at this position. Both the CoMSIA and CoMFA electrostatic maps showed the presence of small red contour in region B, which favoured the presence of partial negative charge in this region. Best active molecule **30** and other higher activity molecules like, **56**, **29**, **26**, **27**, **28**, etc. have groups having heteroatom in

region B, while molecules which lack such heteroatom in this region are observed as least active or lesser active molecules (**43**, **48**, **1**, **2**, **5**, **6**, **50**, etc.). The presence of big blue plot in region C near the substituted side chain attached to the hydrazone shown by CoMSIA contour map and a relatively small blue contour shown in this region by CoMFA contour analysis, favours the presence of electropositive group to improve the activity and binding affinity of the molecules. CoMFA contours also show one small red contour in region C, which is absent in CoMSIA contour map.

### 3.5. Hydrophobic contour map

Hydrophobic contour map from CoMSIA is shown in Fig. 8e. Contour map showed a big yellow contour covering

region A as well as part of central core and the substituted ring, suggesting that increase in hydrophobicity in this region is expected to improve the activity of the molecule. A white contour in a different orientation away from yellow plot is observed in region A, which disfavoured the conformation of hydrophobic substituents towards it and subsequently supports the evidence for importance of conformation of substituted aromatic system in region A for higher activity of molecules. The map also showed yellow plots near the hydrazone and the phenyl ring. Two white plots present in region C near extended side chain suggested increase in activity with substitution of hydrophilic group in this region. The lower activities of molecules **1**, **5**, **6** can be explained from the fact that the conformation of the hydrophobic groups in these inhibitors in region C is not favourable for interaction of the molecules with the protein. For example hydrophobic benzyl group of molecule **35** makes unfavourable contributions to the binding with the protein.

### 3.6. Hydrogen bond donor and acceptor contour map

The contour maps of hydrogen bond donor (Fig. 8f) and acceptor fields (Fig. 8g) describe the spatial arrangement of favourable and disfavoured hydrogen bond interactions to acceptor or donor groups of the target protein. The contour map analysis surrounds most active molecule **30** depicts that cyan contours which are observed opposite the hydrazone hydrogen in the central core and to the benzimidazole hydrogen in region A describe a favourable H-bond to an acceptor group in the protein, while the magenta contours near the benzimidazole nitrogen in region A, hydrazone nitrogen of central core and carbonyl oxygen in region B indicate favourable H-bonds to a hydrogen bond donor structure in the active site.

From the above contour map analysis it appears that improvement in GSK-3 $\beta$  binding affinity can be achieved by substitution having higher ring electronegativity and hydrophobicity in region A. Conformation restriction of substitution at N1 of central core towards sterically favoured side in region A. The ring hydrophobicity and group containing heteroatom which can provide increase in negative character in region B is also an important criterion for improvement in activity towards GSK-3 $\beta$ .

### 3.7. Design of new molecules

The detailed contour analysis of both CoMFA and CoMSIA models enabled us to point out several structural requirements as mentioned in above paragraph for the observed inhibitory activities (Fig. 9). On that basis, the basic skeleton was modified to further improve the inhibition towards GSK-3 $\beta$ . Molecule **30**, the most active GSK-3 $\beta$  inhibitor from the chosen series was used as a reference structure to design new molecules. Structurally, these molecules differ from the reported molecules in that benzimidazole substitution is replaced by a more hydrophobic imidazopyridine substitution, which resulted in the favourable placement of the

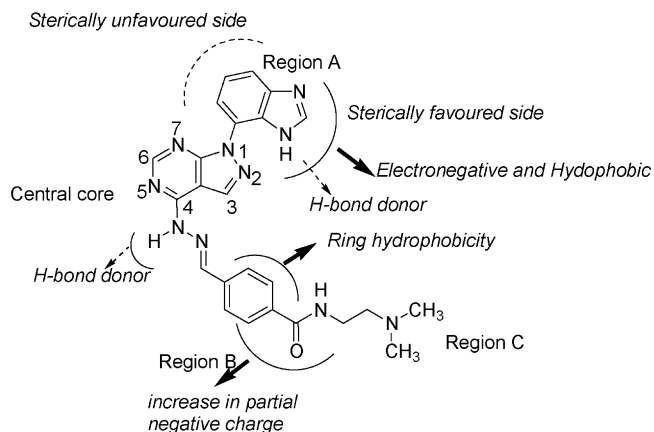


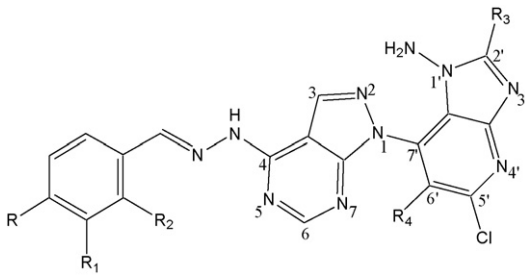
Fig. 9. Structural requirements for pyrazolopyrimidine based GSK-3 $\beta$  inhibitors.

substituent at N1 of the central core in conformationally and sterically favoured region.

A total of about 31 molecules were designed which showed improved pIC<sub>50</sub> values over the reference molecule **30** according to the CoMFA predictions. This was further validated by docking study. The FlexX method of molecular docking was employed to dock the newly designed molecules in the active site of GSK-3 $\beta$ . Based on relative binding affinities from the FlexX score and other docking scores like G\_score, PMF\_score, D\_score and Chem\_score, only 9 molecules were selected out of 31 as new potent ligands (Table 3). Out of these molecules, the molecule with highest docking score, **Des3**, showed that the imidazopyridine nitrogen is making H-bond interaction with Val135 and electrostatic interaction to Asp133 (Fig. 10). These amino acids are found to be important in interacting with previously reported ATP-competitive GSK-3 $\beta$  inhibitors [20]. The amino group at position 1' of the imidazole is seen to make hydrogen bonds with Ile62 and other with neighbouring water molecule. This water molecule on the other side interacts with Thr138 and act as a bridge between ligand and receptor. Electronegative group such as chlorine and fluorine at R<sub>3</sub> position were found to make electrostatic interactions with Arg141. These two interactions are found to be useful in maintaining the conformation of the selective and highly potent designed molecules. Structural analysis of GSK-3 $\beta$  and CDK-2 active site showed that Thr138 of GSK-3 $\beta$  is replaced by Asp86 in CDK-2. Improvement in selectivity towards GSK-3 $\beta$  by molecules showing interaction with Thr138 through bridging water molecule is supported by work done by Bertrand et al. [20]. Thus interaction with Thr138 is an important step towards identification of selective GSK-3 $\beta$  inhibitors. The fact that the designed molecules show this interaction is an indication of their potential selectivity towards GSK-3 $\beta$ . The other important interactions made by **Des3** in the GSK-3 $\beta$  active site include H-bond interaction from N5 of central core pyrimidine ring, NH of the hydrazone with Asp200 and H-bond interactions of the hydrazone at R<sub>2</sub> position with Lys183, Asn186 and Asp200. These designed molecules indeed show



Table 3  
Structures, predicted pIC<sub>50</sub> and docking scores for designed molecules



Mol.	R	R1	R2	R3	R4	CoMFA pIC <sub>50</sub>	CoMSIA pIC <sub>50</sub>	FlexX	G_score	PMF_score	D_score	Chem_score	C-Score
Des1	F	–NHNH <sub>2</sub>	H	F	Cl	9.91	9.80	–30.03	–132.43	–73.16	–125.23	–28.65	5
Des2	H	Cl	–NHNH <sub>2</sub>	Cl	H	10.09	10.00	–32.56	–208.26	–80.45	–132.94	–31.22	5
Des3	F	Cl	–NHNH <sub>2</sub>	F	H	10.32	10.20	–32.59	–209.25	–83.99	–134.30	–31.22	5
Des4	–CONH <sub>2</sub>	H	H	F	Br	10.04	9.95	–28.67	–155.91	–74.76	–132.08	–32.16	5
Des5	Cl	–CN	–NHNH <sub>2</sub>	F	Cl	10.49	10.15	–31.36	–172.28	–22.47	–136.52	–30.96	4
Des6	Cl	–CN	–NH <sub>2</sub>	F	Cl	10.48	10.12	–30.40	–102.78	–51.34	–102.35	–28.26	3
Des7	Cl	–CN	H	F	Cl	10.61	10.57	–26.65	–99.36	–9.36	–76.30	–28.13	2
Des8	–CHO	–CN	H	F	Cl	10.10	10.05	–28.60	–152.56	–66.56	–122.54	–27.62	5
Des9	–CHO	Br	H	F	Cl	10.56	10.20	–26.57	–101.68	–9.36	–78.87	–28.42	2
30						8.80 <sup>a</sup>		–23.12	–165.80	–9.44	–106.39	–30.15	4

<sup>a</sup> Represents actual pIC<sub>50</sub> value.

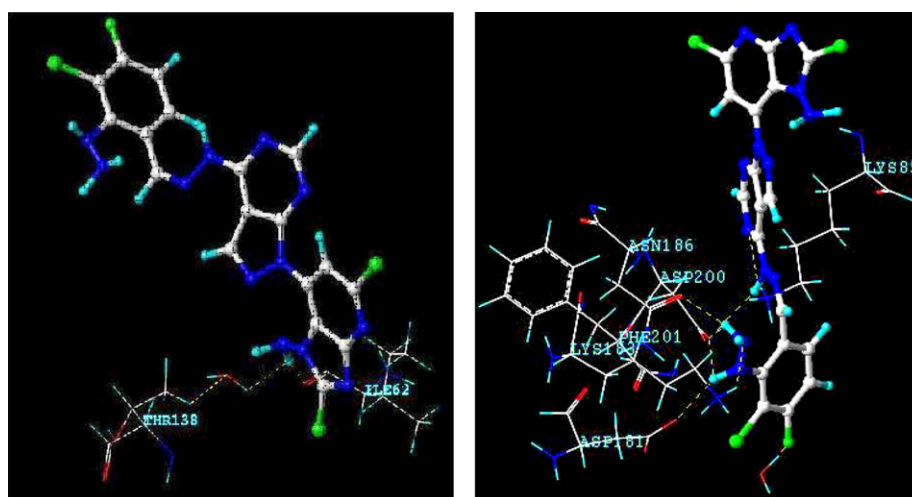


Fig. 10. Interactions of molecule **Des3** with GSK-3β.

better scores in comparison to the reference molecule and interaction for selective in GSK-3β inhibitors indicates that there is a greater chance of the newly designed molecules to be potent and selective towards GSK-3β inhibition.

#### 4. Conclusions

3D-QSARs are widely employed to alter a given structural scaffold so as to develop new molecules that have an improved biological property. CoMFA and CoMSIA methodologies were used to build models for GSK-3β inhibitory activities of the pyrazolopyrimidine derivatives. Based on the detailed

contour analysis, models helped to point out, that improvement in GSK-3β binding affinity can be achieved through conformationally restricted substitution at N1 in region A and the maintenance of the electronegative group to the central core in region B. On the basis of these clues, designed molecules demonstrated better binding affinity in terms of quantitative estimation of binding scores and their interaction with the Thr138 through bridging water molecule is an important criterion for selectivity towards GSK-3 inhibition, which indicates that there is a greater chance of the newly designed molecules to be potent and selective towards GSK-3β inhibition.

## Appendix A. Supplementary data

Supplementary data associated with this article can be found, in the online version, at doi:10.1016/j.jmgm.2006.08.009.

## References

- [1] N. Embi, D.B. Rylatt, P. Cohen, Glycogen synthase kinase-3 from rabbit skeletal muscle. Separation from cyclic-AMP-dependant protein kinase and phosphorylase kinase, *Eur. J. Biochem.* 107 (1980) 519–527.
- [2] A.J. Harwood, Regulation of GSK-3: a cellular multiprocessor, *Cell* 105 (2001) 821–824.
- [3] D.A. Cross, D.R. Alessi, P. Cohen, M. Andjelkovich, B.A. Hemming, Inhibition of glycogen synthase kinase-3 by insulin mediated by protein kinase B, *Nature* 378 (1995) 785–789.
- [4] A. Martinez, A. Castro, I. Dorransoro, M. Alonso, Glycogen synthase kinase 3 (GSK-3) inhibitors as new promising drugs for diabetes, neurodegeneration, cancer and inflammation, *Med. Res. Rev.* 22 (2002) 373–384.
- [5] (a) M. Peifer, P. Polakis, Wnt signaling in oncogenesis and embryogenesis, *Science* 287 (2000) 1606–1609;  
(b) M. Pap, G.M. Cooper, Role glycogen synthase kinase-3 in phosphatidylinositol-3 kinases/Akt cell survival pathway, *J. Biol. Chem.* 273 (1998) 19929–19932.
- [6] (a) T.P. Ciaraldi, S.E. Nikoulina, R.R. Henry, Role of glycogen synthase kinase-3 in skeletal muscle insulin resistance in type-2 diabetes, *J. Diabetes Complicat.* 16 (2002) 69–71;  
(b) S.E. Nikoulina, T.P. Ciaraldi, S. Mudaliar, P. Mohideen, L. Carter, R.R. Henry, Potential role of glycogen synthase kinase-3 in skeletal muscle insulin resistance of type-2 diabetes, *Diabetes* 49 (2000) 263–271;  
(c) S.E. Nikoulina, T.P. Ciaraldi, S. Mudaliar, L. Carter, K. Johnson, R.R. Henry, Inhibition of glycogen synthase kinase 3 improves glucose metabolism in human skeletal muscle, *Diabetes* 51 (2002) 2190–2198.
- [7] S. Ghosh, M. Karin, Missing pieces in the NF- $\kappa$ B puzzle, *Cell* 109 (2002) S81–S96.
- [8] C.J. Phiel, P.S. Klein, Molecular targets of lithium action, *Annu. Rev. Pharmacol. Toxicol.* 41 (2001) 789–813.
- [9] E. Planel, X. Sun, A. Takashima, Role of GSK-3 $\beta$  in Alzheimer's disease pathology, *Drug Dev. Res.* 56 (2002) 491–512.
- [10] J.V. Wauwe, B. Haefner, Glycogen synthase kinase-3 as drug target: from wallflower to center of attention, *Drug News Perspect.* 16 (2003) 557–565.
- [11] A. Martinez, M. Alonso, A. Castro, C. Perez, F. Moreno, First non-ATP competitive glycogen synthase kinase 3 (GSK-3) inhibitors: thiazolidinones (TDZD) as potential drugs for the treatment of Alzheimer's disease, *J. Med. Chem.* 45 (2002) 1292–1299.
- [12] L. Meijer, A.M. Thunnissen, A.W. White, M. Garnier, M. Nikolic, L.H. Tsai, J. Walter, K.E. Cleverley, P.C. Salinas, Y.Z. Wu, J. Biernat, E.M. Mandelkow, S.H. Kim, G.R. Pettit, Inhibition of cyclin-dependent kinases, GSK-3 $\beta$  and CK1 by hymenialdisine, a marine sponge constituent, *Chem. Biol.* 7 (2000) 51–63.
- [13] (a) M. Leost, C. Schultz, A. Link, Y.-Z. Wu, J. Biernat, E.-M. Mandelkow, J.A. Bibb, G.L. Snyder, P. Greengard, D.W. Zaharevitz, R. Gussio, A.M. Senderowicz, E.A. Sausville, C. Kunick, L. Meijer, Paullones are potent inhibitors of glycogen synthase kinase-3 and cyclin dependent kinase 5/p25, *Eur. J. Biochem.* 267 (2000) 5983;  
(b) C. Kunick, C. Lauenroth, M. Leost, L. Meijer, T. Lemcke, 1-Aza-paullone is a selective inhibitor of glycogen synthase kinase-3, *Bioorg. Med. Chem. Lett.* 14 (2004) 413–416.
- [14] L. Meijer, A.L. Skaltsounis, P. Magiatis, P. Polychronopoulos, M. Knockaert, M. Leost, X.P. Ryan, C.A. Vonica, A. Brivanlou, R. Dajani, C. Crovace, C. Tarricone, A. Musacchio, S.M. Roe, L. Pearl, P. Greengard, GSK-3. GSK-3 selective inhibitors derived from Tyrian Purple Indirubins, *Chem. Biol.* 10 (2003) 1255–1266.
- [15] J. Witherington, V. Bordas, S.L. Garland, M.B. Deirdre, D.J. Smith, 6-Heteroaryl-pyrazolo[3,4-*b*]pyridines: potent and selective inhibitors of glycogen synthase kinase (GSK-3), *Bioorg. Med. Chem. Lett.* 13 (2003) 3059–3062.
- [16] H.-C. Zhang, H. Ye, B.R. Conway, C.K. Derian, M.F. Addo, G.-H. Kuo, L.R. Hecker, D.R. Croll, J. Li, L. Westover, J.Z. Xu, R. Look, K.T. Demarest, P. Andrade-Gordon, B.P. Damiano, B.E. Maryano, 3-(7-Azaindolyl)-4-arylmaleimides as potent, selective inhibitors of glycogen synthase kinase-3, *Bioorg. Med. Chem. Lett.* 14 (2004) 3245–3250.
- [17] P.H. Olesen, A.R. Sorensen, B. Urso, P. Kurtzhals, A.N. Bowler, U. Ehrbar, B.F. Hansen, Synthesis and in vitro characterization of 1-(4-aminofurazan-3-yl)-5-dialkylaminomethyl-1H-[1,2,3]triazole-4-carboxylic acid derivatives, *J. Med. Chem.* 46 (2003) 3333–3341.
- [18] D.G. Smith, M. Buffet, A.E. Fenwick, D. Haigh, R.J. Iffe, M. Saunders, B.P. Slingsby, R. Stacey, R.W. Ward, 3-Anilino-4-arylmaleimides: potent and selective inhibitors of glycogen synthase kinase-3 (GSK-3), *Bioorg. Med. Chem. Lett.* 11 (2001) 635–639.
- [19] G.W. Cline, K. Johnson, W. Regittinig, P. Perret, E. Tozzo, L. Xiao, C. Damico, G.I. Shulman, Effects of novel glycogen synthase kinase-3 inhibitors on insulin-stimulated glucose metabolism in Zucker diabetic fatty (fa/fa) rats, *Diabetes* 51 (2002) 2903–2910.
- [20] (a) J.A. Bertrand, S. Thieffine, A. Vulpetti, C. Cristiani, B. Valsasina, S. Knapp, H.M. Kalisz, M. Flocco, Structural characterization of the GSK-3 $\beta$  active site using selective and non-selective ATP-mimetic inhibitors, *J. Mol. Biol.* 333 (2003) 393–407 (<http://www.rcsb.org>, PDB ID – 1PYX.pdb);  
(b) A. Vulpetti, P. Crivori, A. Cameron, J.A. Bertrand, M.G. Brasca, R. D'Alessio, P. Paverello, Structure-based approaches to improve selectivity: CDK2-GSK3 $\beta$  binding site analysis, *J. Chem. Inf. Model.* 45 (2005) 1282–1290.
- [21] (a) D.S. Patel, P.V. Bharatam, New leads for selective GSK-3 inhibition: pharmacophore mapping and virtual screening studies, *J. Comput.-Aided Mol. Des.* 20 (2006) 55–66;  
(b) N. Dessalew, P.V. Bharatam, 3D-QSAR CoMFA study on bisarylmaleimide series as GSK3, CDK2, CDK4 inhibitors: an insight to the criteria for selectivity, submitted for publication.
- [22] A. Martinez, M. Alonso, A. Castro, I. Dorransoro, J.L. Gelpi, F.J. Luque, C. Perez, F. Moreno, SAR and 3D-QSAR studies on thiazolidinone derivatives: exploration of structural requirements of glycogen synthase kinase 3 inhibitors, *J. Med. Chem.* 48 (2005) 7103–7112.
- [23] C. Kunick, K. Lauenroth, K. Wiekling, X. Xie, C. Schultz, R. Gussio, D. Zaharevitz, L. Maryse, L. Meijer, A. Weber, F.S. Jørgensen, T. Lemcke, Evaluation and comparison of 3D-QSAR CoMSIA models for CDK1 CDK5 and GSK-3 inhibition by paullones, *J. Med. Chem.* 47 (2004) 22–36.
- [24] M. Zeng, Y. Jiang, B. Zhang, K. Zheng, N. Zhang, Q. Yu, 3D QSAR studies on GSK-3 inhibition by aloisines, *Bioorg. Med. Chem. Lett.* 15 (2005) 395–399.
- [25] R.D. Cramer III, D.E. Patterson, J.D. Bunce, Comparative molecular field analysis (CoMFA). 1. Effect of shape on binding of steroids to carrier proteins, *J. Am. Chem. Soc.* 110 (1988) 5959–5967.
- [26] G. Klebe, U. Abraham, T. Mietzner, Molecular similarity indices in a comparative analysis of drug molecules to correlate and predict their biological activity, *J. Med. Chem.* 37 (1994) 4130–4146.
- [27] (a) A.J. Peat, J.A. Boucheron, S.H. Dickerson, D. Garrido, W. Mills, J. Peckham, F. Preugschat, T. Smalley, S.L. Schweiker, J.R. Wilson, T.Y. Wang, H.Q. Zhou, S.A. Thomson, Novel pyrazolopyrimidine derivatives as GSK-3 inhibitors, *Bioorg. Med. Chem. Lett.* 14 (2004) 2121–2125;  
(b) A.J. Peat, D. Garrido, J.A. Boucheron, S.L. Schweiker, S.H. Dickerson, J.R. Wilson, T.Y. Wang, S.A. Thomson, Novel GSK-3 inhibitors with improved cellular activity, *Bioorg. Med. Chem. Lett.* 14 (2004) 2127–2130.
- [28] S. Wold, A. Johansson, M. Cochi, 3D QSAR in drug design: theory, methods and applications, in: H. Kubinyi (Ed.), *PLS-Partial Least Squares Projection to Latent Structures*, ESCOM, Lieden, 1993, pp. 523–550.

- [29] M.J.S. Dewar, E.G. Zoebisch, E.F. Healy, J.J.P. Stewart, A new general purpose quantum mechanical molecular model, *J. Am. Chem. Soc.* 107 (1985) 3902–3909.
- [30] SYBYL6.9 is available from Tripos Associates Inc., 1699 S. Hanley Rd., St. Louis, MO 631444, USA.
- [31] M. Rarey, B. Kramer, T. Lengauer, G.A. Kleb, Fast flexible docking method using an incremental construction algorithm, *J. Mol. Biol.* 261 (1996) 470–489.
- [32] G. Jones, P. Willett, R.C. Glen, A.R. Leach, R. Taylor, Development and validation of genetic algorithms for flexible docking, *J. Mol. Biol.* 267 (1997) 727–748.
- [33] I. Muegge, Y.C. Martin, A general and fast scoring function for protein ligand interactions: a simplified potential approach, *J. Med. Chem.* 42 (1999) 791–804.
- [34] I.D. Kuntz, J.M. Blaney, S.J. Oatley, R. Langridge, T.E. Ferrin, A geometric approach to macromolecule ligand interactions, *J. Mol. Biol.* 161 (1982) 269–288.
- [35] M.D. Eldridge, C.W. Murray, T.R. Auton, G.V. Paolini, R.P. Mee, Empirical scoring functions: the development of a fast scoring function to estimate the binding affinity of ligands in receptor complexes, *J. Comput.-Aided Mol. Des.* 11 (1997) 425–445.